Empirical mode decomposition revisited using ordinal pattern concepts

Meryem JABLOUN
Orleans University, PRISME laboratory.
Orleans, France.
meryem.jabloun@univ-orleans.fr

***Abstract*—The empirical mode decomposition (EMD) is a well-known data-driven signal decomposition. It produces a finite number of intrinsic mode functions (IMF) well adapted to Hilbert spectral analysis.**
Since the EMD is not a theoretical approach but rather an iterative algorithm, the question of how the EMD can achieve spectral band separation remains open. Several attempts to experimentally and theoretically explore this issue were addressed. However, to the best of our knowledge, none of them has investigated the EMD from an ordinal pattern point of view.
The purpose of this paper is threefold. First, the EMD limitations are reexamined using the concept of ordinal patterns (OP) of length 3. Second, we propose to incorporate the OP probability distribution into the definition of the mean envelop and the stopping criterion during the sifting process. This turns out to be helpful in reducing mode mixing and thus improves the EMD robustness. Finally, we propose to extend the EMD to different pattern lengths (2, 4, 5, etc). Academic and real-life time series are processed and the results show that the ordinal pattern-based EMD outperforms the classical EMD.

***Index Terms*—Empirical mode decomposition, ordinal pattern, time series.**

I. Introduction

There are a large number of signal decomposition-based methods [1]–[11] that are of great interest in many engineering fields. Among these methods, the empirical mode decomposition (EMD) is a famous approach that was proposed by Huang et al. [1] for recursively decomposing a signal as a sum of intrinsic mode functions (IMF). The IMF are zero mean oscillating functions of data-driven separated spectral bands and they are well-behaved with the Hilbert transform.

Despite the EMD popularity, no existing theory justifies the empirical way the EMD operates. Indeed, EMD has no analytic definition. Only a few studies have contributed to better understanding of some of its specific aspects [12], [13]. We propose to address this issue using the ordinal pattern concept. The potential of such a concept has been recently highlighted in [14], [15].

Given a discrete time-series, the ordinal patterns (OP) of length d are obtained by comparing and ranking d neighbouring sample values. By taking into account 3 consecutive samples x_t, x_{t+1} and x_{t+2}, the extrema identification in the EMD turns out to be a localization of four OPs of length $d = 3$: 132, 231, 312 and 213. The EMD sensitivity to noise, sampling frequency and mode mixing can therefore be linked to the OP distribution (frequency of occurrence of the patterns). This is a fact that has not been previously pointed out in the literature.

We propose to take into account the OP distribution when calculating the average envelop during the sifting process. Indeed, the mixing mode can be reduced by considering the most probable patterns. Moreover, we propose a stop criterion for the sifting process based on the OP theory in order to relax the original IMF definition. Preliminary results show attractive performance compared to the original EMD. Finally, thanks to the OP concept, an extension of the EMD to other OP length is possible and helps emerge new interpretation.

The paper is organized as follows. Section II reformulates the EMD using the OP concept and explores the EMD limitations from an OP point of view. Section III describes how to integrate the OP distribution into the EMD algorithm in order to improve the EMD performance. The extension to other OP lengths is also presented. Section IV presents an illustration and comparison using theoretical and real signals. Finally, conclusions are drawn in Section V.

II. EMD revisited from an OP point of view

This section briefly recalls the EMD algorithm. The aim is then to highlight the potential link between the OP theory and the EMD performance.

A. Classical EMD

The Algorithm 1 summarizes the effective EMD steps. We remind that the stopping criterion of the sifting process was initially set as: the total number of extrema and the number of zero-crossings differ by at most one. As this criterion may lead to no physical meaning IMFs, a Cauchy-based stop criterion is preferred [16] even though the resulting IMFs may fail to satisfy the original IMF definition. Other considerations or modifications of the original EMD have also been proposed in [17], [18] to overcome the EMD limitations. Remind that the EMD is known to be sensitive to noise, sampling frequency and mode mixing of signal components with close frequencies.

B. EMD linked to OP concept

From an OP point of view, the EMD first step can be considered as the localization of four OP of length $d = 3$ among six ($d!$) possible OP (see Fig. 1). These six OP are obtained by ranking the values of successive samples x_t, x_{t+1}

Algorithm 1 EMD

Ensure: $n = 0$.

1: Locate the maxima and minima of a time series x_t.
2: Construct the signals E_{max_t} and E_{min_t} by interpolating these maxima and minima, respectively.
3: Construct a signal average $M_t = \frac{E_{max_t}+E_{min_t}}{2}$.
4: Construct a detail signal $D_t = x_t - M_t$.
5: Sifting process: Repeat steps 1 to 4 by replacing x_t by D_t until a stopping criterion is reached.
6: $n \longleftarrow n+1$ and set the n^{th} IMF$_t = D_t$.
7: Restart steps 1 to 6 by replacing x_t by the residual signal $x_t - D_t$.

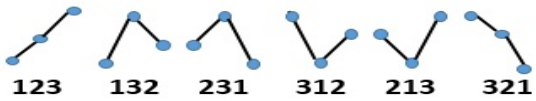

Fig. 1: Six ordinal patterns of length 3 obtained by comparing and ranking three successive sample values: x_t, x_{t+1}, x_{t+2}.

and x_{t+2}. Rank 1 is assigned to the lowest value while rank 3 is assigned to the highest value. We assume that equal values are very rare for any weak stationary process [14]. The OP 231 and its reversal pattern 132 represent the maxima of the considered signal whereas the OP 312 and its reversal pattern 213 represent the minima. Note that the EMD does not take into account the ascending and descending OP: 123 and 321.

C. EMD limitations from an OP point of view

As extrema play an important role in the behaviour of the EMD algorithm, the authors in [13] theoretically determined the extrema rate (the average number of extrema per unit length) for a particular continuous-time signal x_t. This signal x_t was a sum of two pure tone components:

$$x_t = \cos(2\pi t) + a_r \cos(2\pi f_r t + \varphi), \tag{1}$$

where the amplitude ratio $a_r \in \left[10^{-2}, 10^{2}\right]$ and the frequency ratio $f_r \in]0, 1]$. As stated in [13], extrema rate helped explain the mixing mode occurring when $a_r f_r \approx 1$. From an OP of view, one simple but meaningful quantity that can measure similar information as the extrema rate is the turning rate α [15]

$$\text{Turning rate} \qquad \alpha = p_{132}+p_{231}+p_{312}+p_{213} = 1-p_{123}-p_{321}, \tag{2}$$

where p_{Π_i} is the occurring frequency of pattern Π_i of length $d = 3$. This occurring frequency (OP probability distribution) can actually be estimated for any weakly stationary discrete time series as follows [14]:

$$p_{\Pi_i}=\frac{\sharp\{t \mid 0 \leq t \leq N-d+1,\ (x_t, x_{t+1}, x_{t+2}) \text{ is of type } \Pi_i\}}{N-d+1}, \tag{3}$$

where $\sharp$ denotes the cardinal and N is the total number of samples. The turning rate (2) measures the frequencies of turning points (local extrema) and reflects the roughness of the discrete time series. Indeed, $\alpha = 1$ is maximal for an alternating time series (rise and fall). It is equal to $\frac{4}{\pi}\arcsin\left(\frac{1}{2}\right) = \frac{2}{3}$ for a white noise, and it reaches a minimum $\alpha = 0$ for monotonic time series. Note that $\alpha = 1$ is also true for any pure sinusoidal signal sampled at the Nyquist rate, even if this signal is embedded in noise with a signal to noise ratio (SNR) greater than 20 dB.

For lack of space, we only focus on the turning rate (2). However, other interesting quantities can be considered, including the permutation entropy, the up-down equilibrium, the rotation symmetry index and the persistence defined in [14], [15].

Fig. 2a and 2b display the turning rate α (2) as a varying function of the two parameters a_r and f_r of the signal defined by (1). Two different sampling frequencies (F_s) are considered: Nyquist rate (2 Hz) and 100 Hz.

Fig. 2c and 2d illustrate the EMD capacity of separation of the two components of the considered signal (1). This capacity was actually measured in [13] according to the criterion defined by

$$C(a_r, f_r) = \frac{||1^{st}\text{IMF}_t - \cos(2\pi t)||}{||a_r \cos(2\pi f_r t + \varphi)||}, \tag{4}$$

where $||.||$ denotes the L^2 norm.

We also add Fig. 2e and 2f where the total inability of the EMD to decompose the signal (1) is measured using the criterion we define as follows

$$IC(a_r, f_r) = \frac{||1^{st}\ \text{IMF}_t - x_t||}{||a_r \cos(2\pi f_r t + \varphi)||}. \tag{5}$$

As reported in [13] and in agreement with the theory established there, three regions are be noticed from Fig.2d and 2f.

Region I: ($a_r f_r \leq 1$ and $f_r \leq 0.7$) the EMD successfully separates the two modes. Region II: ($a_r f_r \leq 1$ and $f_r \geq 0.7$) the EMD is totally unable to decompose the considered signal. Region III: ($a_r f_r \geq 1$) a partial failure of the EMD to correctly separate the two components. As it can be seen from Fig. 2a, 2c and 2e, these regions edges are actually sensitive to the sampling frequency values.

Regarding the turning rate (2), Region I and Region II are merged in one single region where $\alpha = 0.02$. This value is actually equal to that of the highest frequency mode $cos(2\pi t)$ sampled at $F_s = 100Hz$ ($\alpha = \frac{2f_0}{F_s} = 0.02$ with $f_0 = 1Hz$).

However, the examination of the OP distribution reveals that region I suffers from an imbalance of extrema ($p231 + p132 - (p312 + p213) \neq 0$) whereas region II satisfies the extrema equilibrium ($p231 + p132 - (p312 + p213) \approx 0$). These findings help explain why the EMD acts differently in these two regions. In Region I, EMD will extract the IMFs until the extrema equilibrium is reached. In Region II, no IMF extraction because the signal itself satisfies the IMF definition.

Regarding region III, the turning rate is varying from 0.01 to 0.02, as if the signal is an amplitude modulated sinusuoid with frequency $\frac{1+f_r}{2}$.

To go one step further, since the sampling frequency and the noise may modify the ordinal pattern distribution of the

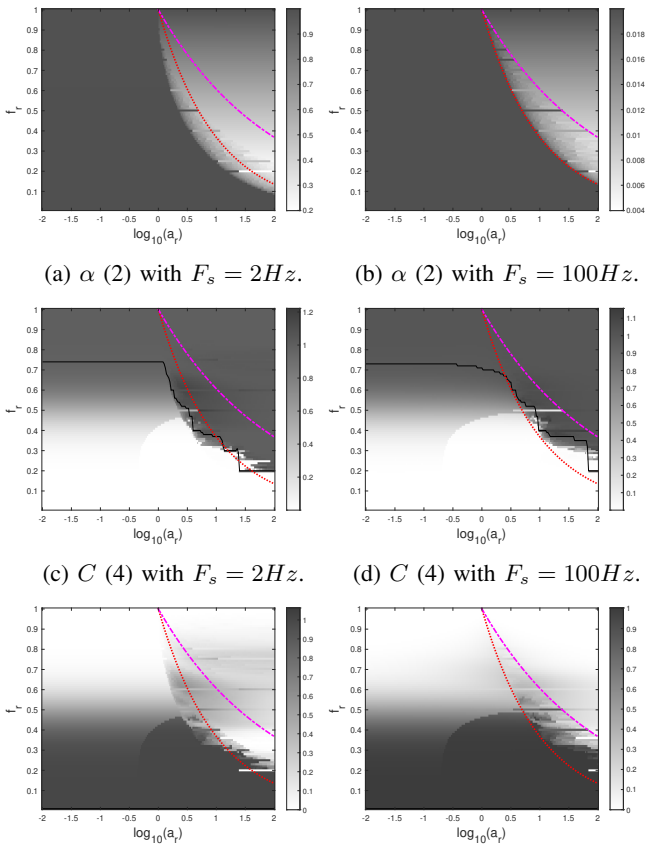

(a) α (2) with $F_s = 2Hz$. (b) α (2) with $F_s = 100Hz$.

(c) C (4) with $F_s = 2Hz$. (d) C (4) with $F_s = 100Hz$.

(e) IC (5) with $F_s = 2Hz$. (f) IC (5) with $F_s = 100Hz$.

Fig. 2: Turning rate α (2) and the EMD Performance (4) and (5) of two-tones signal (1) sampled at (left side) Nyquist rate frequency F_s = 2Hz and (right side) F_s = 100 Hz. Critical curves predicted by continuous time theory in [13] are provided: dotted ($a_r f_r = 1$) and dash-dotted ($a_r f_r^2 = 1$). The black line is the contour $C(a_r, f_r) = 0.98$.

time series, we evaluate α for a pure tone signal ($\cos(2\pi t)$) embedded in noise. Fig. 3 illustrates the variation of α (2) as a function of both F_s and the SNR. As it can be noticed from Fig. 3, the turning rate reaches the maximum 1 at the Nyquist rate $F_s = 2Hz$ for an SNR value greater than 20 dB. However, for example, at SNR = 30 dB, this turning rate reaches a minimum at $F_s = 20Hz$ and it reaches the typical value $\frac{2}{3}$ of white noise at $F_s = 200Hz$. In addition, a plateau $\alpha = \frac{2}{3}$ is noticed for higher F_s whatever the SNR ratio. This again allows us to understand the EMD behaviour with respect to sampling frequency and the noise level. Indeed, at a high sampling rate, α measures a high amount of noise-related patterns, the EMD algorithm will first extract noise-related IMFs before reaching an amount of patterns that actually reflect the pure tone itself.

D. Open questions

The EMD performance seems to be closely linked to the ordinal pattern distribution, and in particular to the patterns

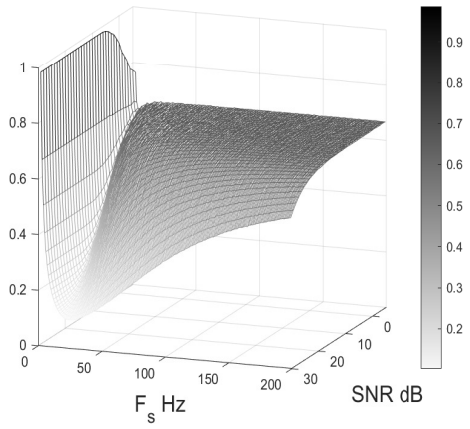

Fig. 3: The turning rate α (2) varies as a function of the sampling frequency and the SNR. For each SNR value, 30 Monte Carlo simulations of a 100 periods of a pure sinusoid $cos(2\pi t)$ embedded in noise are generated.

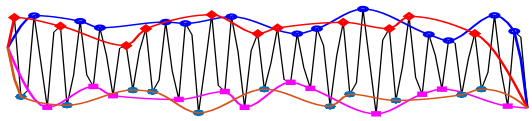

Fig. 4: Four curves: (blue) E_{132_t} , (red) E_{231_t}, (magenta) E_{312_t} and (yellow) E_{213_t} obtained by separate interpolation of maxima and minima issued from the same pattern.

representing extrema: 312, 231, 132 and 213. These patterns are, however, far from being the most probable ones. Can taking into account the ascending and descending patterns improve the EMD performance? If so, what will the best combination of patterns and how can this combination be incorporated into the EMD algorithm? Furthermore, is it possible to define an EMD based on the localization of patterns of length greater or less than 3? In the next section, we propose one way but not the only way, to answer these questions.

III. Proposed OP-based EMD

We propose a new version of the EMD algorithm based on the OP concept, our aim being to take into account the OP distribution. The modification of the original EMD is reported in Algorithm 2 and detailed in three points in the following. First, we propose to distinguish between contribution of patterns and their reversal patterns as shown in Fig. 4. Each pattern is considered apart when building interpolated envelops. For example, we identify all the points x_t of type pattern 132 and then interpolate them to form the curve E_{132_t}. We use the same procedure with its reversal pattern 231 to obtain E_{231_t}. We proceed in the same manner with patterns 312 and 213 to construct E_{312_t} and E_{213_t}, respectively. We propose also to construct two other curves E_{123_t} and E_{321_t} from the localization of ascending and descending patterns 123 and 321, respectively. As shown in Fig. 5a, the idea is to

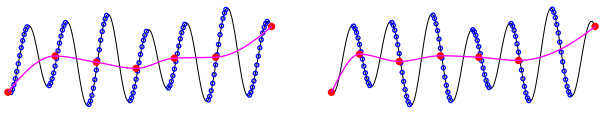

(a) Segments of pattern 123. (b) Segments of pattern 321.

Fig. 5: Two curves: E_{123_t} and E_{321_t} constructed by interpolating the centers of segments of successive samples of ascending and descending patterns.

identify the centers of segments formed by successive samples of pattern 123 and to interpolate them in order to obtain a curve E_{123_t}. We proceed similarly for the pattern 321 (see Fig. 5b).

We define the average envelop as the sum of all the E_{Π_t} weighted by the their pattern distribution:

$$M_t = \sum_{i=1}^{d!=6} p_{\Pi_i} E_{\Pi_t}. \tag{6}$$

We perform the sifting process until a stopping criterion is reached. We can use the following OP-based stopping criterion:

$$\text{Persistence} \qquad |p_{123} - p_{321}| \leq 1 - \epsilon \tag{7}$$

The persistence (7) was defined in [15]. It seems to be suitable for balanced processes and it highlights hidden periodicity. The performance of the proposed OP-based EMD will be compared to the classical EMD in the next section.

Algorithm 2 OP-based EMD

Ensure: $n = 0$.

1: Localize the six OPs of length 3 of a finite discrete time series x_t and evaluate the OP distribution.
2: Construct four curves $E_{\Pi_{i_t}}$ by interpolating the extrema of each pattern, separately.
3: Construct two curves $E_{\Pi_{i_t}}$ from the ascending pattern and the descending one as shown in Fig. 5a and 5b.
4: Construct a signal average $M_t = \sum_{i=1}^{d!=6} p_{\Pi_i} E_{\Pi_{i_t}}$.
5: Construct a detail signal $D_t = x_t - M_t$.
6: Sifting process: Repeat steps 1 to 5 by replacing x_t by D_t until a stopping criterion (7) is reached.
7: $n \longleftarrow n + 1$ and set the n^{th} IMF$_t = D_t$.
8: Restart steps 1 to 7 by replacing x_t by the residue $x_t - D_t$.

Very importantly, the proposed OP-based EMD method can be easily extended to an OP of length $d \neq 3$. Indeed, all the steps of the Algorithm 2 can be defined for $d = 2$, $d = 4$, $d = 5$ etc. For example, for $d = 2$, there are only two ordinal patterns (ascending) 12 and (descending) 21 with probability distribution $p(x_t < x_{t+1}) = p_{12}$ and $p(x_t > x_{t+1}) = p_{21}$. For $d = 4$, there will be 4!=24 patterns to be localized and 24 interpolated curves. However, a necessary condition will be that the sample number $N >>> d!$ to ensure an unbiased estimation of the OP distribution.

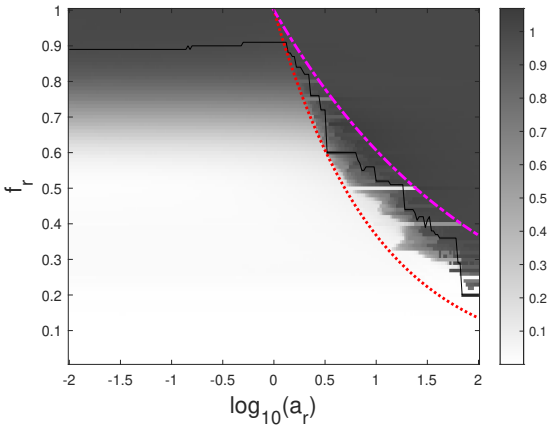

Fig. 6: OP-based EMD performance: separating capacity of a sum of two two-tones signal (1) sampled at $F_s = 100$ Hz. Critical curves predicted by continuous time theory in [13] are provided: dotted ($a_r f_r = 1$) and dash-dotted ($a_r f_r^2 = 1$). The black line is the contour $C(a_r, f_r) = 0.98$.

IV. Results and Discussion

In order to illustrate performance of the proposed OP-based EMD and to compare it with the classical EMD, we consider three signals

- the academic signal defined by (1) and composed of the sum of two non-modulated frequency components. The sampling frequency is $F_s = 100$ Hz.
- a (odd and zero-mean) square waveform of time period $T = 10$ms sampled at $F_s = 1$KHz. Before dealing with this square waveform, we should remind that such an analog signal has a Fourier series expansion and an infinite number of harmonics:

$$x_t \approx \sum_{n=0}^{\infty} \frac{4}{(2n+1)\pi} sin(2\pi(2n+1)\frac{t}{T}). \tag{8}$$

  And, to avoid the aliasing problem, this signal is passed through an anti-aliasing filter.
- a real-data: the well-known monthly sunspot series re-sampled to obtain $F_s = 1$ year^{-1} (http://sidc.oma.be).

Fig. 6 depicts the separating criterion (4) for the OP-based method using the signal defined by (1). The stopping criterion (7) is used. As one can notice from Fig. 2d, the region of successful separation of the two modes is highly increased ($f_r < 0.9$): the mixing mode is reduced.

Fig. 7 shows the first two IMFs extracted from the square waveform using the EMD and the OP-based EMD to be superimposed to the first two theoretical harmonics (C_{th_t}). The mean error ($||C_{th_t} - IMF_t||^2$), measured for the High Frequency component, is equal to 2.19 using the OP-based EMD and it is equal to 2.39 using the classical EMD. For the Low frequency component, this error is 1.46 and 1.74, respectively.

Finally, Fig. 8 illustrates the processing of the sunspot data using the OP-based EMD with $d = 2$ and $d = 3$. The very

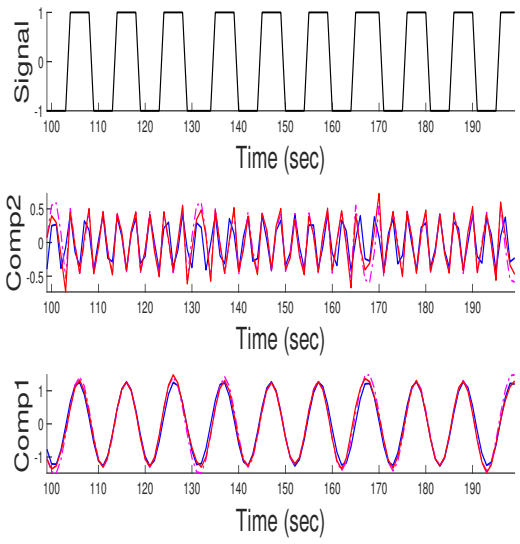

Fig. 7: (black line) Analog (odd and zero mean) Square waveform. The first two IMF extracted using (red line) the OP-based EMD (d=3) and (magenta line) the classical EMD superimposed to the (blue line) first two theoretical harmonics.

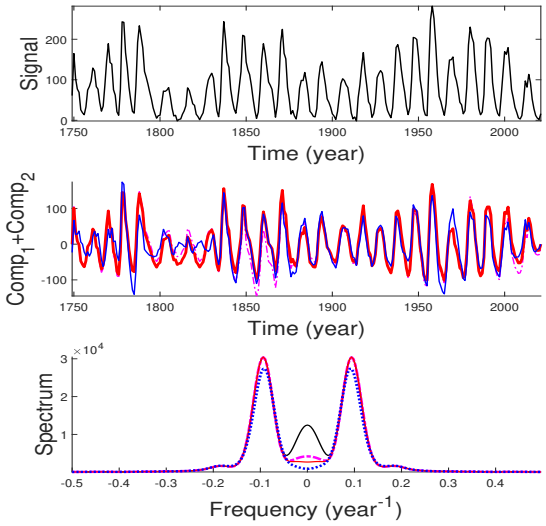

Fig. 8: (black line) Sunspot time series. (red line) and (blue line) the sum of the first two extracted IMF using the OP-based EMD (d=3) and (d=2), respectively. (magenta line) The sum of the first two IMF extracted using the classical EMD. The spectrum of this sum is superimposed to (black line) the raw data spectrum.

low frequency content seems to be better removed from the sum of the two IMF extracted using the OP-based EMD with $d = 2$.

V. Conclusions

The well-known signal decomposition method, EMD, is revisited using the concepts of ordinal pattern of length 3. We then proposed a new OP-based formulation of the EMD where the pattern distribution is involved into the sifting process. The proposed OP-based EMD reduces the mixing mode and it hence outperforms the classical EMD when applied to time series with close frequency components. In addition, this proposed OP-based EMD can be extended to any ordinal pattern length. The potential of the OP-based EMD with ordinal pattern of length greater than 3 will be deeply addressed in future work.

References

[1] N. E. Huang, Z. Shen, S. R. Long, M. C. Wu, H. H. Shih, Q. Zheng, N.-C. Yen, C. C. Tung, and H. H. Liu, "The empirical mode decomposition and the Hilbert spectrum for nonlinear and non-stationary time series analysis," *Proc. of the R. Soc. of London. Series A: Math., Phys. and Eng. Sciences*, vol. 454, no. 1971, pp. 903–995, Mar. 1998.

[2] J. S. Smith, "The local mean decomposition and its application to EEG perception data," *Journal of The R. Soc. Interface*, vol. 2, no. 5, pp. 443–454, Dec. 2005.

[3] M. Feldman, "Time-varying vibration decomposition and analysis based on the Hilbert transform," *Journal of Sound and Vibration*, vol. 295, no. 3-5, pp. 518–530, Aug. 2006.

[4] M. G. Frei and I. Osorio, "Intrinsic time-scale decomposition: time–frequency–energy analysis and real-time filtering of non-stationary signals," *Proc. of the R. Society A: Math., Phys. and Eng. Sciences*, vol. 463, no. 2078, pp. 321–342, Feb. 2007.

[5] J. Gilles, "Empirical Wavelet Transform," *IEEE trans. on sig. proc.*, vol. 61, no. 16, pp. 3999–4010, Aug. 2013.

[6] J. Zheng, J. Cheng, and Y. Yang, "A rolling bearing fault diagnosis approach based on LCD and fuzzy entropy," *Mechanism and Machine Theory*, vol. 70, pp. 441–453, Dec. 2013.

[7] K. Dragomiretskiy and D. Zosso, "Variational Mode Decomposition," *IEEE trans. on sig. proc.*, vol. 62, no. 3, pp. 531–544, Feb. 2014.

[8] R. Beresik, "Hilbert-Huang transform and its application in seismic signal processing," in *2016 New Trends in Signal Processing (NTSP)*. Demanovska Dolina: IEEE, Oct. 2016, pp. 1–6.

[9] F. Zhou, L. Yang, H. Zhou, and L. Yang, "Optimal averages for non-linear signal decompositions—Another alternative for empirical mode decomposition," *Signal Processing*, vol. 121, pp. 17–29, Apr. 2016.

[10] S. Chen, X. Dong, Z. Peng, W. Zhang, and G. Meng, "Nonlinear Chirp Mode Decomposition: A Variational Method," *IEEE trans. on sig. proc.*, vol. 65, no. 22, pp. 6024–6037, Nov. 2017.

[11] J. Harmouche, D. Fourer, F. Auger, P. Borgnat, and P. Flandrin, "The Sliding Singular Spectrum Analysis: A Data-Driven Nonstationary Signal Decomposition Tool," *IEEE trans. on sig. proc.*, vol. 66, no. 1, pp. 251–263, Jan. 2018.

[12] P. Flandrin, G. Rilling, and P. Goncalves, "Empirical mode decomposition as filter bank," *IEEE sig. proc. Letters*, vol. 11, no. 2, pp. 112–114, Feb. 2004.

[13] G. Rilling and P. Flandrin, "One or two frequencies? The Empirical Mode Decomposition Answers," *IEEE trans. on sig. proc.*, vol. 56, no. 1, pp. 85–95, Jan. 2008.

[14] C. Bandt and F. Shiha, "Order patterns in time series," *Journal of Time Series Analysis*, vol. 28, no. 5, pp. 646–665, Sep. 2007.

[15] C. Bandt, "Small order patterns in big time series: A practical guide," *Entropy*, vol. 21, no. 6, p. 613, Jun. 2019.

[16] G. Wang, X.-Y. Chen, F.-L. Qiao, Z. Wu, and N. E. Huang, "On intrinsic mode function," *Advances in Adaptive Data Analysis*, vol. 02, no. 03, pp. 277–293, Jul. 2010.

[17] N. Pustelnik, P. Borgnat, and P. Flandrin, "Empirical mode decomposition revisited by multicomponent non-smooth convex optimization," *Signal Processing*, vol. 102, pp. 313–331, Sep. 2014.

[18] N. Qiao, L.-h. Wang, Q.-y. Liu, and H.-q. Zhai, "Multi-scale eigenvalues Empirical Mode Decomposition for geomagnetic signal filtering," *Measurement*, vol. 146, pp. 885–891, Nov. 2019.